Centrum voor Wiskunde en Informatica

REPORT*RAPPORT*

MAS

Modelling, Analysis and Simulation

Modelling, Analysis and Simulation

On the numerical solution of diffusion-reaction equations with singular source terms

M. Ashyraliyev, J.G. Blom, J.G. Verwer

REPORT MAS-E0512 JULY 2005

CWI is the National Research Institute for Mathematics and Computer Science. It is sponsored by the Netherlands Organization for Scientific Research (NWO).
CWI is a founding member of ERCIM, the European Research Consortium for Informatics and Mathematics.

CWI's research has a theme-oriented structure and is grouped into four clusters. Listed below are the names of the clusters and in parentheses their acronyms.

Probability, Networks and Algorithms (PNA)

Software Engineering (SEN)

Modelling, Analysis and Simulation (MAS)

Information Systems (INS)

P.O. Box 94079, 1090 GB Amsterdam (NL)
Kruislaan 413, 1098 SJ Amsterdam (NL)
Telephone +31 20 592 9333
Telefax +31 20 592 4199

ISSN 1386-3703

On the numerical solution of diffusion-reaction equations with singular source terms

ABSTRACT
A numerical study is presented of reaction-diffusion problems having singular reaction source terms, singular in the sense that within the spatial domain the source is defined by a Dirac delta function expression on a lower dimensional surface. A consequence is that solutions will be continuous, but not continuously differentiable. This lack of smoothness and the lower dimensional surface forms an obstacle for numerical discretization, including amongst others order reduction. In this paper the finite volume approach is studied for linear and nonlinear test models. The aimed application field lies in developmental biology from which a test model is used for numerical illustration.

2000 Mathematics Subject Classification: 65M12, 65M20, 65L05.
1998 ACM Computing Classification System: G.1.7, G.1.8.
Keywords and Phrases: Reaction-diffusion equations, singular source terms, finite volume methods.
Note: Work carried out within theme MAS1.

On the Numerical Solution of Diffusion-Reaction Equations with Singular Source Terms

M. Ashyraliyev and J.G. Blom and J.G. Verwer
CWI
P.O. Box 94079, 1090 GB Amsterdam, The Netherlands

ABSTRACT
A numerical study is presented of reaction-diffusion problems having singular reaction source terms, singular in the sense that within the spatial domain the source is defined by a Dirac delta function expression on a lower dimensional surface. A consequence is that solutions will be continuous, but not continuously differentiable. This lack of smoothness and the lower dimensional surface forms an obstacle for numerical discretization, including amongst others order reduction. In this paper the finite volume approach is studied for linear and nonlinear test models. The aimed application field lies in developmental biology from which a test model is used for numerical illustration.

2000 Mathematics Subject Classification: Primary: 65M12, 65M20, 65L05.

1998 ACM Computing Classification System: G.1.7 and G.1.8.
Keywords and Phrases: Reaction-diffusion equations, singular source terms, finite volume methods.
Note: Work carried out within theme MAS1.

1. Introduction

In this paper we discuss the numerical solution of diffusion-reaction problems

$$u_t = L(u) + f \tag{1.1}$$

with a singular reaction source term f. Singular means here that within the domain $\Omega \subset \mathbb{R}^d$ of L the source f is defined by a Dirac delta function expression on a lower dimensional surface $\Gamma \subset \Omega$ rather than on the whole of Ω. A consequence is that the solution u is not a solution on Ω in the classical sense because across Γ the solution u will be continuous, but not continuously differentiable. This lack of smoothness and the lower dimension of Γ forms an obstacle for numerical discretization. With any numerical method one has the obvious question how to represent Γ and how to discretize f on a common grid. For finite-difference methods this question is studied in detail in [12] using regularization ideas. Regularization in the sense that the Dirac delta function expression is approximated by a source giving a small but regular support allowing standard finite difference schemes for L. In a close vicinity of Γ the lack of smoothness of u will still be felt with regularization, in the sense that in general the convergence order in the maximum norm is at best equal to one [12].

Our main application field for the current research is in developmental biology where mass conservation is important. In this paper we therefore follow the finite volume approach based on the integral form of (1.1). We consider this approach also more natural than the finite

difference one directly based on the differential form, since for the integral form the treatment of the Dirac delta function expression is mathematically clear. However, also with the finite volume approach the problem of lack of smoothness remains, causing order reduction from two to one for the standard second-order spatial discretization scheme. In spite of this order reduction the schemes we discuss do perform well for our application.

The paper is organized as follows. In Section 2 we start with linear 1D and 2D test models, simple and yet significant enough to reveal the essence of a singular source. In this section the emphasis lies on boundary value problems. In Section 3 we turn to test models having a nonlinear source and here the emphasis lies on initial-boundary value problems. In both these sections we illustrate our findings numerically. Section 4 is devoted to the test problem from biochemistry describing a simple developmental regulatory network. The paper is concluded with a summary of our findings in Section 5.

2. Linear test models

2.1 Boundary value problems

We begin with the boundary value problem for the 1D equation

$$-u_{xx} = \phi(x)\,, \qquad 0 < x < 1\,, \tag{2.1}$$

provided with the homogeneous Dirichlet conditions $u(0) = 0, u(1) = 0$. This simple 1D problem acts as a nice test model. In spite of its simplicity it already reveals essential numerical properties for the Dirac delta function source $\phi(x) = \delta(x - \bar{x})$, $\bar{x} \in (0, 1)$. For this ϕ the solution u of (2.1) is no longer a classical solution in the sense that it can be explicitly substituted in the differential equation. It can be determined however by the Green's function expression [2]

$$u(x) = \int_0^1 G(x, y)\phi(y)dy\,, \qquad G(x, y) = \begin{cases} x\,(1 - y)\,, & 0 \le x \le y\,, \\ y\,(1 - x)\,, & y < x \le 1\,. \end{cases} \tag{2.2}$$

Using the delta function property $\int_0^1 f(x)\delta(x - \bar{x}) = f(\bar{x})$ insertion of $\phi(x) = \delta(x - \bar{x})$ gives

$$u(x) = \begin{cases} x\,(1 - \bar{x})\,, & 0 \le x \le \bar{x}\,, \\ \bar{x}\,(1 - x)\,, & \bar{x} < x \le 1\,. \end{cases} \tag{2.3}$$

Note that u is continuous but not continuously differentiable over $[0, 1]$.

The finite volume approach In this section we will analyze the standard cell-centered discretization scheme for (2.1) obtained through the finite volume approach. For u smooth (sufficiently differentiable) this scheme converges with second order in the maximum norm. However, for the solution defined by the Dirac delta function the scheme becomes locally inconsistent near $\bar{x}$ resulting in a maximum norm order reduction from two to one for the global error. For the sake of insight we will analyze this reduction phenomenon from two points of view, viz. by introducing modified equations as in backward error analysis and by examining the local truncation error as in common forward error analysis.

Let $h = 1/m$ where m is the number of uniform grid cells $\Omega_i = [(i-1)h, ih]$ for $i = 1, \ldots, m$ covering $[0, 1]$. Let $x_i = (i - 1/2)h$ denote the cell center of Ω_i. The finite volume approach for (2.1) amounts to first integrating (2.1) over Ω_i and dividing by the cell volume,

$$\frac{\int_{\Omega_i} -u_{xx}(x)dx}{\int_{\Omega_i} dx} = \frac{\int_{\Omega_i} \phi(x)dx}{\int_{\Omega_i} dx}\,, \qquad i = 1, \ldots, m\,,$$

followed by applying the divergence (Gauss) theorem,

$$-\frac{u_x(x_{i+1/2})}{\int_{\Omega_i} dx} + \frac{u_x(x_{i-1/2})}{\int_{\Omega_i} dx} = \frac{\int_{\Omega_i} \phi(x)dx}{\int_{\Omega_i} dx}\,, \qquad i = 1,\ldots,m\,, \tag{2.4}$$

followed by choosing a difference approximation for u_x and computing the integrals, either exact or by a quadrature rule. After incorporating the boundary conditions this procedure then results in the aimed discretization scheme.

Correct application of the divergence theorem generally impedes existence and integrability of u_{xx} which does not hold with a Dirac delta function for ϕ.[1)] To circumvent this problem we will assume, for the sake of analysis only, that we are solving a modified equation defined by a modified source term associated to $\delta(x-\bar{x})$. More specifically, we will associate $\delta(x-\bar{x})$ with a class of source functions $\phi(x)$ leading to twice continuously differentiable solutions u and which are equivalent with $\delta(x-\bar{x})$ in the sense that

$$\int_{\Omega_i} \phi(x)dx = \int_{\Omega_i} \delta(x-\bar{x})dx\,, \qquad i = 1,\ldots,m\,. \tag{2.5}$$

The divergence theorem is then applicable for these twice continuously differentiable solutions and, furthermore, assuming exact integration or a proper quadrature rule, the ϕ-integrals in (2.4) are computed as if the source is the Dirac delta function. Hence the resulting difference scheme remains unaltered.

In addition to (2.5) we will further assume that any ϕ considered converges to the Dirac delta function with $\mathcal{O}(h)$ in the sense that

$$\int_0^1 G(x,y)\big(\phi(y) - \delta(y-\bar{x})\big)dy = \mathcal{O}(h)\,. \tag{2.6}$$

Due to (2.2) this requirement immediately leads to first-order convergence of the exact modified solution u to the sought exact solution. This in turn implies first-order convergence of the numerical solution to the sought solution if we have first-order h-convergence of the numerical solution to the assumed modified solution. Below we will illustrate this line of thinking which is reminiscent of backward error analysis as used in numerical linear algebra or numerical differential equations, see e.g. [4].

To set up the difference scheme let us assume that $\bar{x} \in (x_{j-1/2}, x_{j+1/2})$ for a certain $j = j(h)$ at a distance ch of the cell center x_j, i.e., $\bar{x} = x_j + ch$ with $-1/2 < c < 1/2$. Then due to (2.5), (2.4) becomes

$$-\frac{u_x(x_{i+1/2})}{h} + \frac{u_x(x_{i-1/2})}{h} = \frac{\delta_{ij}}{h}\,, \qquad i = 1,\ldots,m\,, \tag{2.7}$$

where δ_{ij} is the Kronecker delta symbol. Next, let $w_i, i = 1,\ldots,m$, denote the numerical solution for $u(x_i)$ resulting from approximating $u_x(x_{i+1/2})$ in (2.7) by $\big(u(x_{i+1}) - u(x_i)\big)/h$, etc. The Dirichlet boundary values are accounted for by extrapolation to auxiliary values $w_0 = 2u(0) - w_1$, $w_{m+1} = 2u(1) - w_m$ and by insertion of w_0 and w_{m+1} for $i = 1$ and $i = m$, respectively. If we then assemble the w_i in the grid function $w = (w_1,\ldots,w_m)^T$, we get as

[1)] Solution (2.3) forms an exception. For this solution the divergence theorem appears to hold over the cell Ω_i containing $\bar{x}$.

numerical scheme the $m \times m$ symmetric linear system [2)]

$$-Aw = b\,, \quad A = \frac{1}{h^2}\begin{pmatrix} -3 & 1 & & & \\ 1 & -2 & 1 & & \\ & \ddots & \ddots & \ddots & \\ & & 1 & -2 & 1 \\ & & & 1 & -3 \end{pmatrix}, \quad b = \frac{1}{h}\begin{pmatrix} 0 \\ \cdot \\ 1 \\ \cdot \\ 0 \end{pmatrix}, \tag{2.8}$$

where b has zero entries except at entry j. The inverse of the difference matrix is bounded uniformly in $h = 1/m$, defining $w = A^{-1}b$ uniquely as the aimed numerical solution.

Let $u_h = (u(x_1), \ldots, u(x_m))^T$ denote the restriction of $u(x)$ to the grid. As discussed above, the numerical solution w can be interpreted as an approximation to u_h for a twice differentiable modified solution u defined by an appropriate source function ϕ satisfying (2.5). Likewise, once constructed, w may also be directly compared to the actually sought solution lying at a maximum norm distance $\mathcal{O}(h)$ to any appropriate modified solution.

Error analysis through modified solutions Associating a uniquely determined numerical solution with different exact modified solutions for the sake of analysis is the central idea of backward error analysis. This line of thinking may enhance insight in the numerical discretization procedure or, as in our case, even justify the discretization procedure. Here we are in the special situation of being able to find the numerical solution and exact modified solutions in closed form. One can easily check that

$$w_i = \begin{cases} x_i(1 - x_j)\,, & i = 1, \ldots, j\,, \\ x_j(1 - x_i)\,, & i = j+1, \ldots, m\,, \end{cases} \tag{2.9}$$

solves (2.8). This numerical solution differs from solution (2.3) only in that $\bar{x}$ is replaced by x_j, revealing a small shift in the peak and an error at all grid points. In terms of $\bar{x}$ and ch, with $-1/2 < c < 1/2$, we have

$$w_i = \begin{cases} x_i(1 - \bar{x}) + cx_i h\,, & i = 1, \ldots, j\,, \\ \bar{x}(1 - x_i) - c(1 - x_i)h\,, & i = j+1, \ldots, m\,, \end{cases} \tag{2.10}$$

immediately showing $\mathcal{O}(h)$ maximum norm convergence. For $c = 0$, i.e., with the singular point $\bar{x}$ located in the center of cell Ω_j, the scheme returns the sought solution exactly.

Next consider by way of example the continuous source function

$$\phi(x) = \begin{cases} 0\,, & 0 \le x \le x_j - h/2\,, \\ \frac{4}{h^2}(x - x_j + h/2)\,, & x_j - h/2 \le x \le x_j\,, \\ \frac{4}{h^2}(x_j - x + h/2)\,, & x_j \le x \le x_j + h/2\,, \\ 0\,, & x_j + h/2 \le x \le 1\,, \end{cases} \tag{2.11}$$

[2)] The values -3 at the corner entries are due to the fact that we have chosen a cell-centered grid and have Dirichlet boundary values. With a vertex-centered grid (boundary points as cell centers) the common stencil would result with -2 at the corner entries. See Section I.5.3 in [5] for accuracy aspects.

which satisfies (2.5) and results in the twice continuously differentiable modified solution

$$u(x) = \begin{cases} x(1-x_j)\,, & 0 \le x \le x_j - h/2\,, \\ x(1-x_j) - \frac{2}{3h^2}(x - x_j + h/2)^3\,, & x_j - h/2 \le x \le x_j\,, \\ x_j(1-x) - \frac{2}{3h^2}(x_j - x + h/2)^3\,, & x_j \le x \le x_j + h/2\,, \\ x_j(1-x)\,, & x_j + h/2 \le x \le 1\,. \end{cases} \tag{2.12}$$

On the grid this modified solution is closer to the numerical solution (2.9) than the sought one as it should be. The u_h and w coincide at all grid points except at x_j where the difference is $h/12$. Observe that (2.11) can be interpreted as a regularized form of the singular Dirac delta function as discussed in [12]. Contrary to the approach followed here, in [12] such regularized forms are explicitly used and implemented in the used difference schemes.

Error analysis through the truncation error Following the common approach of forward error analysis we will next examine the convergence of (2.8) to the sought solution u by analyzing the local truncation error σ and global error e defined by

$$\sigma = -Au_h - b\,, \qquad e = u_h - w\,.$$

There holds $-Ae = \sigma$ so that $\|e\|_\infty \le \|A^{-1}\|_\infty \|\sigma\|_\infty$. Hence if $\|\sigma\|_\infty = \mathcal{O}(h^2)$ we immediately have second-order convergence in view of the uniform boundedness of $\|A^{-1}\|_\infty$. However, for the current solution (2.3) we find

$$\sigma = \Big(0, \ldots, 0, \frac{-c}{h}, \frac{c}{h}, 0, \ldots, 0\Big)^T\,, \tag{2.13}$$

with nonzero entries for cell j and $j+1$, respectively. Here it is assumed that $\bar{x}$ lies at the right of x_j so that $0 \le c < 1/2$. With $\bar{x}$ at the left the nonzero entries shift to cells $j-1, j$. For $c = 0$, i.e., with the singular point located in the center of cell Ω_j, a zero truncation error results and hence in this special case the scheme returns the exact solution (2.3). In all other cases $\|\sigma\|_\infty = \mathcal{O}(h^{-1})$ so that convergence cannot be concluded when the standard argument sketched above is followed.

Through a more subtle local truncation error analysis the correct maximum norm $\mathcal{O}(h)$ convergence can be proven however, gaining two powers of h. A similar situation generally occurs with Dirichlet boundary conditions due to the cell-centered location of x_1 and x_m half a distance h away from the boundary. For a general smooth solution we then would have $\sigma_1 = \mathcal{O}(1), \sigma_m = \mathcal{O}(1)$. In [5], Section I.5.3, it is shown that we then still can expect second-order convergence (with a sufficiently smooth source) due to a favourable local error cancellation and we adopt here the method of proof of [5] to show first-order convergence with σ given by (2.13) using the following ansatz: the local truncation error can be decomposed as $\sigma = -Ar + \xi$ such that the grid functions r, ξ are componentwise $\mathcal{O}(h)$. This would immediately prove first-order convergence since the global error then satisfies $e = r - A^{-1}\xi$. The ansatz is verified as follows. Put $\xi = 0$ and $r = h\alpha$. We then have to verify that such a grid function α exists and satisfies $\alpha = \mathcal{O}(1)$ componentwise. The result is

$$\alpha_i = \begin{cases} \frac{1-2i}{2m}\,c\,, & i = 1, \ldots, j\,, \\ \frac{2m-2i+1}{2m}\,c\,, & i = j+1, \ldots, m\,, \end{cases} \tag{2.14}$$

which completes the proof. Observe that since $\xi = 0$ we have $e = h\alpha$ connecting this expression with (2.9) through $w = u_h - h\alpha$.

Example 2.1 As a second illustration of the $\mathcal{O}(h)$ convergence of the cell-centered scheme we consider a slight extension of the 1D test model (2.1), viz.,

$$-u_{xx} + u = \delta(x - \bar{x}) \,, \qquad 0 < x < 1 \,, \tag{2.15}$$

again with homogeneous Dirichlet boundary conditions. This problem does have as solution

$$u(x) = \begin{cases} \frac{\sinh(1-\bar{x})\sinh(x)}{\sinh(1)} \,, & 0 \le x \le \bar{x} \,, \\ \frac{\sinh(1-x)\sinh(\bar{x})}{\sinh(1)} \,, & \bar{x} \le x \le 1 \,. \end{cases}$$

Figure 2.1 shows u (left plot, solid line) for $\bar{x} = 0.3$ along with the cell-centered solution for $h = 1/20$ (o-marks). The plot at the right nicely reveals the anticipated first-order convergence ($\|u_h - w\|_\infty$ versus m in log-log scale).

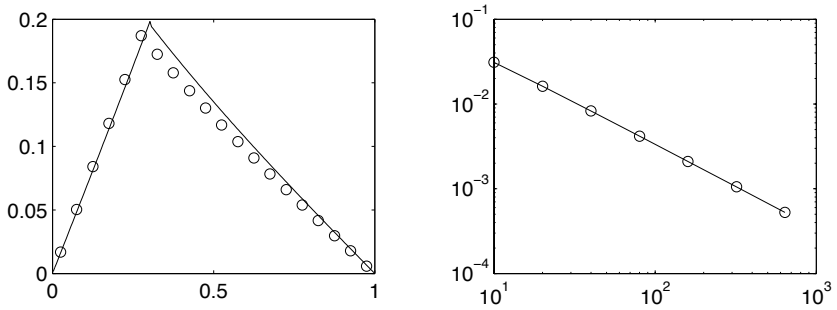

Figure 2.1: Numerical illustration for problem (2.15) with $\bar{x} = 0.3$.

Example 2.2 An interesting 2D test model used in [12] is the Poisson equation

$$-\Delta u = \delta(\Gamma, x, y) \,. \tag{2.16}$$

Here the source denotes the Dirac delta function along a curve Γ defined by

$$\int_{\mathbb{R}^2} \delta(\Gamma, x, y)\, dxdy = \int_\Gamma d\gamma \,, \tag{2.17}$$

with co-ordinate γ on Γ. As in the 1D test model, solution u is continuous but not continuously differentiable across Γ so that the divergence theorem cannot be correctly applied. However, by arguing with assumptions similar to (2.5), (2.6), the divergence theorem is correctly applied for twice differentiable modified solutions and the resulting 2D cell-centered scheme (the 2D counterpart of (2.8)) will again result in first-order convergence to the sought solution u.

Using a uniform $m \times m$ grid the 2D counterpart of (2.8) reads

$$-(A \otimes I + I \otimes A)w = b \,, \tag{2.18}$$

where $\otimes$ is the direct matrix (Kronecker) product. The entries b_k of the vector $b \in \mathbb{R}^{m\times m}$ are associated to grid cells Ω_{ij} with values emanating from the boundary conditions and the source $\delta(\Gamma, x, y)$. Considering the source contribution, let $\Gamma_{ij} = \Gamma \cap \Omega_{ij}$ and $|\Gamma_{ij}|$ the length of Γ_{ij}. Then, assuming exact integration of the integral along Γ, from (2.17) and the finite volume approach follows that either

$$b_k = |\Gamma_{ij}|/h^2 \tag{2.19}$$

or $b_k = 0$ (considering only the source term contribution). Because upon intersection $|\Gamma_{ij}|$ is proportional to h, b_k is then proportional to $1/h$ or equal to zero, similar as in the 1D case.

For the circle $\Gamma = \{(x, y) : x^2 + y^2 = r^2\}$ problem (2.16) has the radial symmetric solution [12]

$$u(x,y) = \begin{cases} u_\Gamma\,, & x^2+y^2 \le r^2\,, \\ u_\Gamma - r\log\left(r^{-1}\sqrt{(x^2+y^2)}\right), & x^2+y^2 \ge r^2\,, \end{cases} \tag{2.20}$$

where u_Γ is a given constant value on Γ. For $u_\Gamma = 1, r = 1/2$ we have applied scheme (2.18) on the square $-1 < x, y < 1$ with Dirichlet boundary values prescribed from (2.20). Figure 2.2 shows the corresponding u and nicely illustrates the first-order convergence of (2.18). The right figure plots $\|u_h - w\|_\infty$ versus m in log-log scale. We have used (nearly) exact integration along Γ (for the circle this is straightforward).

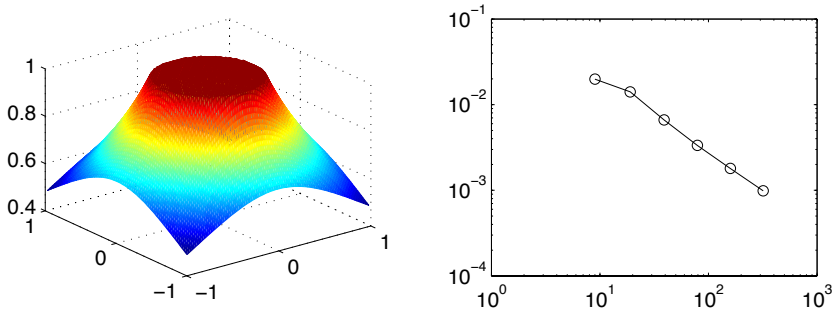

Figure 2.2: Numerical illustration for problem (2.16)-(2.20).

Remark 2.3 No finite solution exists when using the two-dimensional Dirac delta function at a point. To see this, consider (now) on the unit square, $-\Delta u = \delta(x - 1/2, y - 1/2)$ with homogeneous Dirichlet boundary values. Introduce the uniform vertex-centered (cell centers at the boundary) $m \times m$ grid with grid size $h = 1/(m + 1)$ and assume m odd. Applying as above the finite volume approach over all internal $h \times h$ grid cells then leads to a linear system $\mathcal{A}w = b$ of type (2.18) where A is defined as in (2.8), except that at the corner points -3 is replaced by -2 (the standard stencil for homogeneous Dirichlet boundary values). Further, vector b has all its components equal to zero, except at entry $k = (m^2 + 1)/2$

associated to the center point $(1/2, 1/2)$. Here $b_k = 1/h^2$ due to

$$\int_{\mathbb{R}^2} \delta(x - 1/2, y - 1/2) = 1 \, .$$

Since $\mathcal{A}$ is symmetric, its inverse satisfies $\mathcal{A}^{-1} = XD^{-1}X^T$ with eigenvector matrix X and eigenvalue matrix D. Consequently, $w_k = (r_k \cdot D^{-1} r_k^T)/h^2$ where r_k is the k-th row of X. Using the known expressions for the eigenvectors and eigenvalues [5], Section III.6.2, we then find the expression

$$w_k = \sum_{\text{odd}\, i,j=1}^{m} 1/\mu_{ij} \, , \qquad \mu_{ij} = h^{-2}\big(\sin^2\big(\frac{\pi i h}{2}\big) + \sin^2\big(\frac{\pi j h}{2}\big)\big) \, , \qquad h = \frac{1}{m+1}$$

for the numerical solution at the center point $(1/2, 1/2)$. Figure 2.3 plots the numerical solution on the 39×39 grid (left plot) and w_k as a function of increasing m-values (right plot; $m = 10 \cdot 2^l - 1$, $l = 0, 1, \ldots, 10$). Even on fine grids w_k is of moderate size, but it is obvious that $w_k \to \infty$ for $m \to \infty$. Since the w_k-sequence is defined by a convergent scheme we conclude that no finite solution exists. It can be shown analytically that $w_k \sim (2\pi)^{-1} \log(m)$ for $m \to \infty$ confirming the growth shown in the figure.

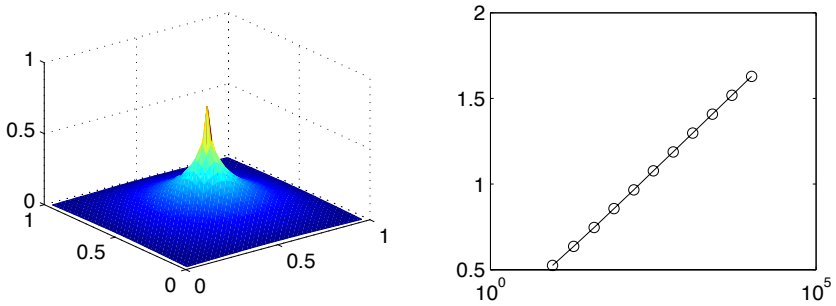

Figure 2.3: Numerical illustration for the ill-posed 2D problem from Remark 2.3.

Remark 2.4 On any fixed grid no matter how fine, the strength of the Γ-source will vanish upon shrinking Γ due to (2.17). The strength is kept by scaling (dividing) the source by $|\Gamma|$, the length of Γ. Such scaling will replace (2.19) by $b_k = (|\Gamma_{ij}|/|\Gamma|)/h^2$ and hence if Γ lies in one or only a few grid cells we have, respectively, $b_k = 1/h^2$ as if we have a point source, or $b_k \approx 1/h^2$. This situation will lead to irregular peak behavior upon grid refinement when initially Γ lies in one cell. First, as long as Γ lies in this same one cell, the peak height will increase, cf. Remark 2.3. Then, when Γ becomes distributed over a few cells, the height will decrease till it eventually settles down when there are enough intersections. Needless to say that this type of irregular behavior may also occur with unscaled sources, but then with a factor h smaller. Small scaled sources simply require finer grids to achieve the same level of absolute errors. Scaling is often wanted, see Section 4 where it is also used in our biological application.

2.2 Time dependent problems

The step from boundary value problems to time-dependent problems with singular source terms is not large. Consider in a spatial domain $\Omega \in \mathbb{R}^d$ the general, constant coefficient,

second order, linear test model

$$u_t = Lu + \phi(\underline{x}), \qquad t > 0, \quad \underline{x} \in \Omega, \tag{2.21}$$

provided with an initial function $u(\underline{x}, 0)$ at time zero, appropriate boundary conditions for $t > 0$, and a singular source term ϕ. The spatial discretization and source treatment through the finite volume approach goes essentially the same as in the boundary value case.

For any volume or grid box $V \in \mathbb{R}^d$ it starts from the integral form

$$\frac{\partial}{\partial t} \frac{\int_V u \, d\underline{x}}{\int_V d\underline{x}} = \frac{\int_V Lu \, d\underline{x}}{\int_V d\underline{x}} + \frac{\int_V \phi(\underline{x}) \, d\underline{x}}{\int_V d\underline{x}}.$$

For the u_t-integral term we will suppose the midpoint quadrature rule approximating the left-hand side by a value $w_V'(t)$ say where $'$ denotes d/dt. As in the boundary value case we will interpret ϕ to be a source function giving rise to a twice continuously differentiable solution $u(\underline{x}, t)$ so that we may apply the divergence theorem for Lu. This ϕ is then supposed to satisfy a counterpart of (2.5) for the singular source under consideration, so that we end up with a semi-discrete central difference scheme identical to that for the singular source.

The scheme takes the generic form of a linear, constant coefficient ODE system

$$w'(t) = Aw(t) + b, \qquad t > 0, \quad w(0) = w_0, \tag{2.22}$$

the solution of which can be expressed as

$$w(t) = e^{At} w(0) + (e^{At} - I) A^{-1} b. \tag{2.23}$$

If the exponential operator satisfies $\exp(At) \to 0$ for $t \to \infty$, this solution results in the steady state $w = -A^{-1}b$ for $t \to \infty$. The spatial error analysis for finite t is almost identical to the analysis for the stationary case. The local truncation error σ and global error e are now defined by

$$\sigma(t) = u_h'(t) - Au_h(t) - b, \qquad e(t) = u_h(t) - w(t),$$

and come together in the global error equation

$$e'(t) = Ae(t) + \sigma(t), \qquad t > 0, \quad e(0) = u_h(0) - w(0).$$

Assuming bounds on the exponential matrix, $e(t)$ then can be expressed in bounds on $\sigma(t)$. Hereby one should use a refined error analysis similar as shown above to cater for local order reduction coming from a singular source. Such a refined error analysis can be found in [5], Section I.5.3, for a similar reduction coming from the boundary. These results carry over to reduction caused by singular sources.

The final assumption is that a counterpart of (2.6) is satisfied so that the modified solution lies at a maximum norm distance $\mathcal{O}(h)$ of the solution u generated by the singular source. First-order maximum norm convergence of $w(t)$ for the modified solution then results automatically in first-order maximum norm convergence to u. What then remains is to turn the continuous time solution $w(t)$ in a fully discrete solution by numerical time integration (method of lines). There exists a great deal of choices of integrators, depending on issues like stiffness, stability, consistency and efficiency [5]. In the next section we will pick one in a numerical illustration for a time-dependent problem with a nonlinear source.

3. Nonlinear test models

We will next consider a nonlinear extension of the linear test models discussed in the previous section. Our aim is to include singular nonlinear reaction terms, singular in the sense that the chemical reactions are confined to a lower dimensional surface Γ in the space domain $\Omega \subset \mathbb{R}^d$, similar as in the previous section. The nonlinear test model has the time-dependent form

$$u_t = Lu + \delta(\Gamma, \underline{x})\, R(\underline{x}, t, u)\,, \qquad \underline{x} \in \Omega\,, \quad t > 0\,. \tag{3.1}$$

The definition of L is here of secondary importance. For simplicity of presentation we assume that Lu is the linear elliptic form $Lu = \nabla \cdot (D\nabla u)$ with $D \in \mathbb{R}^{d\times d}$ diagonal and dependent on $\underline{x}$ only. The source term is supposed to satisfy the Dirac delta function relation [12]

$$\int_{\mathbb{R}^d} \delta(\Gamma, \underline{x}) R(\underline{x}, t, u) d\underline{x} = \int_\Gamma R(\underline{x}(\gamma), t, u) d\gamma\,, \tag{3.2}$$

with co-ordinate γ on Γ. The dependent variable $u(\underline{x}, t)$ is supposed to represent s concentrations, hence u is a vector $u = (u_1, \ldots, u_s)$ and accordingly the nonlinear vector function $R(\underline{x}, t, u)$ has also s components. Providing (3.1) with appropriate initial and boundary conditions yields the initial-boundary value problem we wish to solve.

The focus of our investigation lies in the singular source term treatment and for this purpose we again take $d = 2$ with $\Omega = (-1, 1)^2$ and assume for space discretization the finite volume approach with centered finite differences on a uniform $m \times m$-grid with grid size $h = 2/m$, completely similar to the linear case presented in Example 2.2. This space discretization leads to the following nonlinear counterpart of system (2.22),

$$w'(t) = Aw(t) + b\big(t, w(t)\big)\,, \qquad t > 0\,, \quad w(0) = w_0\,. \tag{3.3}$$

With a smooth source term defined on the whole of Ω we would have second-order consistency. However, the singular source term will lead to first-order consistency and what remains to show is how this term enters the nonlinear vector function $b(t, w)$. Consider a grid cell Ω_{ij} and recall the derivation of Example 2.2. If $\Gamma \cap \Omega_{ij} = \emptyset$, the corresponding contributions to b are zero. If $\Gamma \cap \Omega_{ij} \neq \emptyset$, these contributions are unequal zero and are obtained from the first-order approximation

$$|\Gamma_{ij}|\, R\big(\underline{x}_{ij}, t, u(\underline{x}_{ij}, t)\big) \approx \int_{\Gamma_{ij}} R\big(\underline{x}(\gamma), t, u\big) d\gamma\,.$$

Associating the index pair (i, j) with an index k for b, we thus get

$$b_k = |\Gamma_{ij}|\, R(\underline{x}_k, t, w_k)/h^2\,. \tag{3.4}$$

The computation of b thus goes essentially the same as in the linear case with regard to the singular source term treatment, the only difference being that b_k is nonlinear in the cell-center value w_k. This might complicate the numerical integration in time, but should form otherwise no obstacle for obtaining a fully discrete numerical solution.

Remark 3.1 Two invariants for u are positivity (componentwise non-negativity) and mass conservation. We distinguish molecular and spatial mass conservation. The first emanates from the mass action law of chemical kinetics [5] and amounts to the existence of constant,

nonnegative weight vectors $v = (v_1, \ldots, v_s)^T$, such that for any solution of the ODE system $u' = R(\underline{x}, t, u)$ the inner product $v^T u(\underline{x}, t)$ is constant in time (the molecular mass defined by v). Trivially, this holds iff $v^T R(\underline{x}, t, w) = 0$ for any $w \in \mathbb{R}^s$. The spatial conservation depends on the boundary conditions, as usual. Combining these two properties will reveal conservation of the total mass

$$M(t) = \int_\Omega v^T u(\underline{x}, t) d\underline{x}$$

associated to a given v. To see this, we compute

$$M'(t) = \int_\Omega v^T \Big(\nabla \cdot (D \nabla u) + \delta(\Gamma, \underline{x})\, R(\underline{x}, t, u) \Big) d\underline{x}\,,$$

and due to (3.2), molecular mass conservation, and the divergence theorem, we have

$$M'(t) = \int_\Omega v^T \Big(\nabla \cdot (D \nabla u) \Big) d\underline{x} = \sum_{i=1}^{s} \int_{\delta\Omega} (D \nabla u_i) \cdot \mathbf{n}\, d\underline{x}$$

and get as usual that the fluxes over the boundary determine conservation of the total mass.

Since we use the finite volume approach for spatial discretization this argument applies to any grid box and the standard result will then be that for the semi-discrete solution $w(t)$, $M(t)$ will be approximated over the space grid (to at least first-order in space) by a linear functional $M_h(t) = Q^T w(t)$ which mimics the time evolution of $M(t)$. In particular, $M_h(t)$ will be constant in time if this holds for $M(t)$ and any Runge-Kutta or linear multi-step method will mimic this in the time integration because these methods conserve linear invariants, see [4], Section IV.1.5.

Positivity of (3.1) under discretization depends on the spatial discretization and the time integration. The central scheme we favor here for approximating (3.1) by (3.3) is positive [5], Section I.7. To guarantee unconditional positivity in time, that is, for any step size $\tau > 0$, we are bound to the first-order implicit Euler method [5]. We prefer however to sacrifice this guarantee in favor of more time accuracy and will instead use a second-order IMEX version of the second-order BDF method.

Example 3.2 We will solve (3.1)-(3.4) for the reaction system

$$R(u) = \begin{cases} -k u_1 u_2 + k u_2^2 \\ -k u_2^2 + k u_1 u_2 \end{cases} \qquad \big(2[u_2] \overset{k}{\rightleftharpoons} [u_1] + [u_2] \big)$$

The corresponding ODE system $u' = R(u)$ has the exact solution

$$u_1(t) = \frac{s_0}{2} \frac{1 - \alpha + 2\alpha\, e^{-s_0 k t}}{1 - \alpha + \alpha\, e^{-s_0 k t}}\,, \quad u_2(t) = s_0 - u_1(t)\,,$$

where $\alpha = (2u_1(0) - s_0)/s_0$ and $s_0 = u_1(t) + u_2(t)$ which is constant in time (linear invariant). For $t \to \infty$ the ODE solution (u_1, u_2) approaches the steady state $(s_0/2, s_0/2)$ exponentially fast. Here we take $k = 1$ and a finite time interval since we are interested in transient behavior. For the PDE system we choose for the diffusion part the Laplace operator, $u_1(x, y, 0) = 0$ and $u_2(x, y, 0) = s_0 = 1$ for initial functions, and homogeneous Neumann

(no flux) for boundary conditions. Due to the no-flux condition, $u_1(x,y,t)+u_2(x,y,t) \equiv s_0$. For Γ we define two circles $(x-x_0)^2+(y-y_0)^2 = r^2$ with respectively the center points $(.5,-.5),(-.5,.5)$ and radii $.05,.25$. As in Example 2.2 the $|\Gamma_{ij}|$ are computed (nearly) exactly.

For reasonable grid sizes h the parabolic linear part Aw in (3.3) will readily be stiff. The reaction constant $k=1$ does not introduce stiffness for the nonlinear term $b(t,w)$, but due to its singular nature this term has entries proportional to $|\Gamma_{ij}|/h^2 \sim 1/h$ which causes it to be mildly stiff. For time integration we can therefore use the following implicit-explicit (IMEX) version of the BDF2 scheme [5], Section IV.4,

$$w_{n+1} = \frac{4}{3}w_n - \frac{1}{3}w_{n-1} + \frac{2}{3}\tau A w_{n+1} + \frac{2}{3}\tau\big(2b(t_n,w_n) - b(t_{n-1},w_{n-1})\big)\,. \tag{3.5}$$

This IMEX scheme treats the linear part implicitly and the nonlinear part explicitly and thus avoids nonlinear equation solutions. It does retain the second-order of consistency of BDF2 and if we take τ proportional to h it can deal with the modest stiffness introduced by the singular source. For the first integration step, the similar IMEX form of implicit Euler [5] is used to provide the additional starting value w_1.

For $h = 2/199$ and $\tau = 1/200$ Figure 3.1 shows the computed u_1-field at $t = 0.025$ (left), 0.05 (middle), 0.1 (right). Recall that at time $t = 0$ the u_1-field is zero and note the difference in vertical scaling to see that on the current time interval both sources survive diffusion. The growth along the larger circle is larger due to the greater source strength.

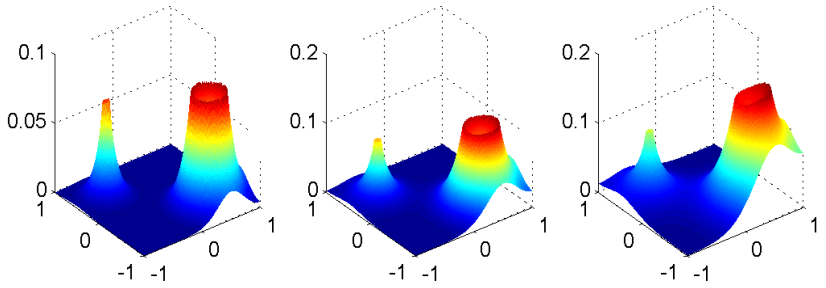

Figure 3.1: Numerical illustration for the problem from Example 3.2.

4. A test model from developmental biology

Our aimed application field for these reaction-diffusion models with singular source terms lies in developmental biology, or more precisely in the simulation of body-plan formation. A small number of genes is responsible for the developmental process from a fertilized eggcell to an individual. These genes, or the gene products, interact via a regulatory network and diffuse through the organism. The idea is that the different types of body segmentation during the development can be explained by 'rewiring' the regulatory network.

We have developed a model [1] for simulating regulatory networks that is capable of quantitatively reproducing spatial and temporal expression patterns in developmental processes. The model is a generalization of the standard connectionist model (see, e.g., [3, 6, 7, 8, 9]) used for modelling genetic interactions. It distinguishes between the genetic regulation which takes place inside the cells (species g) and the diffusion of the signalling pathway components (species c) through the organism. Mathematically speaking this amounts to

a continuum-discrete hybrid model where discrete objects exchange species with the surrounding environment modelled as a continuum. Inside the cells one has genetic regulation and decay (biochemical reactions). In [1] and in this paper we assume that the concentration inside these cells is homogeneous (no diffusion). Outside the cells species only diffuse and decay. The exchange of the signalling pathway components between the cells and the extracellular matrix is described by a secretion/absorption function. This function models membrane processes giving rise to reaction source terms modelled with the Dirac delta function (3.2) defined on the surface of the cells.

In this section we numerically solve a model from [1] inspired by the blastoderm stage of development of *Drosophila* (fruit-fly, see, e.g. [6]). Since in the initial phase of *Drosophila* the cells are in a syncytium (no cell membrane), secretion/absorption between intracellular and extracellular is instantaneous, which in our model is reflected by a large value for the constant coefficient α.

The (discrete) equations describing the *intracellular* processes read [1]

$$\frac{dg_i^a(t)}{dt} = R_a \Phi(\sum_{b=1}^{N_g} W^{ab} g_i^b) - \lambda_a g_i^a - \alpha \frac{\int_{\partial V_i} (g_i^a - c^a(\underline{x}(S), t)) dS}{|\partial V_i|}. \tag{4.1}$$

The variable g_i^a stands for the concentration of gene product a within biological cell i, with $i = 1, \ldots, N_c$ (being the number of biological cells). N_g is the number of different gene products. So, we have $N_c \times N_g$ equations (4.1). $W = (W^{ab})$ is a matrix of genetic regulatory coefficients whose elements characterize the influence of gene b on gene a. R_a is the maximum rate of synthesis from gene a, λ_a is the decay rate of gene a, and Φ is a sigmoid function with range [0,1] (0: no production, 1: saturation) for which we use the Hill curve with coefficient two:

$$\Phi(x) = \frac{z^2}{(0.5)^2 + z^2}, \quad z = \max(0, x). \tag{4.2}$$

The last term in (4.1) models the contribution of the secretion/absorption process integrated over the surface ∂V_i of cell i. Note that the interaction between the gene products g in all cells is induced by the same regulatory matrix. External influences, like the secretion/absorption process, govern the level of the concentrations g_i^a for the different cells.

The diffusion-reaction model for the species in the *extracellular* matrix is modelled by the following N_g equations

$$\frac{\partial c^a(\underline{x}, t)}{\partial t} = \nabla.(D_a \nabla c^a(\underline{x}, t)) - \lambda_a c^a(\underline{x}, t) + \sum_{j=1}^{N_c} V_j \frac{\delta(\partial V_j, \underline{x})}{|\partial V_j|} \alpha \left(g_j^a(t) - c^a(\underline{x}, t) \right), \tag{4.3}$$

where V_j is the volume of the biological cell j, D_a is the diffusion parameter of gene a and c^a stands for the extracellular concentration of gene product a. Note that here the Dirac delta function $\delta(\partial V_j, \underline{x})$ is present in the same setting as in (3.2). Since in the *Drosophila* embryo the level of expression of genes is, approximately, a function only of position along the anterior-posterior (A-P) axis, equations (4.3) can be reduced to a system of (pseudo) one-dimensional equations (the biological cells are still 3D) with the spatial dependency in z-direction, where $z \in [0, Z]$ [1].

4.1 Numerical approximation

For the spatial discretization of the (pseudo) one-dimensional analog of equations (4.3) we use cell-centered second-order finite volume discretization similar as in Section 2.1.1 and Section 2.2. Assume that the biological cells are uniformly distributed, equally sized spherical cells. Let z_i be the location of the center of bio-cell i and r_c its radius. Let $h = Z/N_z$ be the mesh size, where N_z is the number of grid cells. Then for all grid cells $[z_l - h/2, z_l + h/2]$ we have to compute the contribution of the secretion/absorption operator restricted to that grid cell. A lengthy calculation gives

$$\sum_{j=1}^{N_c} \frac{1}{4\pi r_c^2} \left(2 \int_0^{\pi} \int_{\theta_{j_l}}^{\theta_{j_r}} r_c^2 \sin\psi \; d\theta \; d\psi \right) \alpha (g_j^a - \bar{c}_l^a),$$

where $\bar{c}_l^a$ is the average concentration value given by $\bar{c}_l^a = \frac{1}{h} \int_{z_l - \frac{h}{2}}^{z_l + \frac{h}{2}} c^a(z,t) dz$, $r_c = \frac{Z}{N_c} \sqrt{\frac{3\gamma}{2\pi}}$, with γ being the ratio between the intracellular volume and the total volume and

$$\theta_{j_l} = \arccos \frac{\partial_{j_l}}{r_c}, \quad \theta_{j_r} = \arccos \frac{\partial_{j_r}}{r_c}, \quad [\partial_{j_l}, \partial_{j_r}] = [-r_c, r_c] \cap [z_l - z_j - \frac{h}{2}, z_l - z_j + \frac{h}{2}]$$

(arccos mapping $[-1,1]$ onto $[-\pi, 0]$). The discretized version for the l-th grid cell then reads

$$\frac{dc_l^a}{dt} = \frac{D_a \frac{c_{l+1}^a - c_l^a}{h} - D_a \frac{c_l^a - c_{l-1}^a}{h}}{h} - \lambda_a c^a + \alpha \frac{w_\gamma}{h} \sum_{j=1}^{N_c} \frac{\theta_{j_r} - \theta_{j_l}}{\pi} (g_j^a - c_l^a), \tag{4.4}$$

where $c_l^a = \bar{c}_l^a + O(h^2)$ is the pointwise approximation to $c^a(z,t)$ at (z_l, t) and $w_\gamma = \frac{\gamma Z}{N_c}$.

Note that the integral in (4.1) is just the sum over all grid cells overlapping bio-cell i. The system of $N_z \times N_g$ ODEs (4.4) coupled with the $N_c \times N_g$ ODEs for the biochemical reactions in the bio-cells (4.1) is solved with the IMEX-BDF2 time integrator (3.5). Only the diffusion operator in (4.4) is treated implicitly, which effectively decouples the two systems in each timestep. Note that the weight factor w_γ ensures that the secretion/absorption term is handled in a mass conservative way. The spatial and temporal discretization preserve mass as well (see Remark 3.1).

4.2 Simulation results

We will demonstrate the behaviour of the hybrid model with a simple artificial regulatory network. It is given by three genes with the following mechanism: gene 1 activates gene 2, and gene 2 inhibits gene 3. The latter two also have auto-activation. This leads to the following regulatory matrix

$$W = \begin{pmatrix} 0 & 0 & 0 \\ 4 & 1 & 0 \\ 0 & -4 & 10 \end{pmatrix}.$$

The other model parameters are given by $R = (1,1,1)$, $\lambda = (5, 0.25, 0.2)$, and $D = (0.15, 0.001, 0.0001)$. The domain length is given by $Z = 1$ and we take 10 uniformly distributed bio-cells that occupy 10% of the total volume ($\gamma = 0.1$, $w_\gamma = 0.01$). Finally, the secretion/absorption factor $\alpha = 1000$.

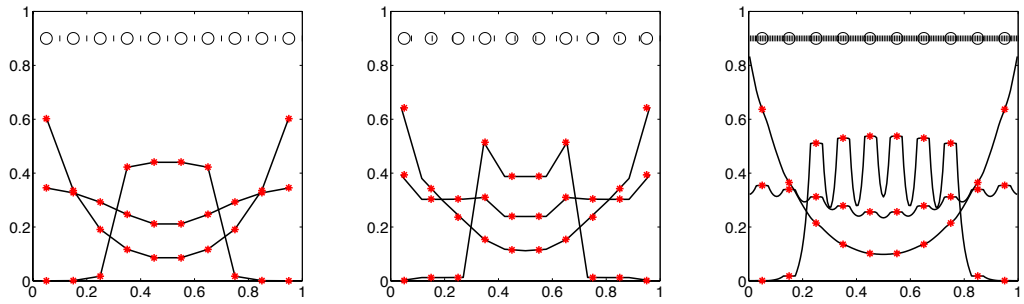

Figure 4.1: Simulations for various numbers of grid cells, left: 10, middle: 13, right: 159. The upper part of the pictures shows the position and size of the bio-cells (○) and the grid cells. The solid lines in the plots show the concentration values of the extracellular species c (boundary values for species 1, 2, and 3 are approximately 0.85, 0.3, and 0.0, respectively), the stars the concentrations of g inside the bio-cells.

The boundary conditions for c are homogeneous Neumann, except for gene product 1 where a concentration of 0.85 is prescribed on both sides. The concentration values of both c and g are initially 0.05.

In Figure 4.1 the simulation results are shown for three different spatial meshes for time $t = 25$ (steady-state), obtained with a highly accurate time integration so that the spatial errors dominate. We used the constant step size $\tau = 10^{-3}$ satisfying the explicit stability constraint $\alpha\tau \leq 1$. In the first experiment each bio-cell lies in a grid cell. Results with this configuration can essentially also be obtained with the standard connectionist model (cf. [1]), since the concentration values inside (g_i^a) and outside (c^a) the bio-cells are approximately the same ($\alpha = 1000$). The plot on the right however shows that the hybrid model predicts also the difference in intensity between the bio-cells and the concentration in the extracellular matrix which is of course dependent on the ratio between the diffusion and reaction coefficients. Finally, the middle plot shows that the relative placement of the grid nodes and the bio-cells can have a large influence on the solution for a coarse mesh. Note, however, that all three experiments give globally the same information if one is only interested in which region which gene product dominates.

Finally, to study the numerical convergence when $h \to 0$, we have solved (4.1), (4.4) on a very fine mesh and have used the resulting numerical solution as the reference solution to study the spatial convergence behaviour. In Figure 4.2 we plot the L_2 norm of the difference between the reference solution and the numerical solutions on the meshes with different grid sizes ranging from 10^{-1} to 0.24×10^{-4} for the extracellular concentration c for the three different genes. We observe a convergence order slightly larger than one instead of two. The order reduction, due to the presence of the delta function in (4.3), does confirm our findings in the previous sections.

5. Concluding remarks

In this paper we studied reaction-diffusion problems with singular reaction source terms. Such sources do contain or are defined by a Dirac delta function living on a lower dimensional surface. The finite volume approach was examined for linear and nonlinear test models. These models do have continuous solutions, but solutions are not continuously differentiable.

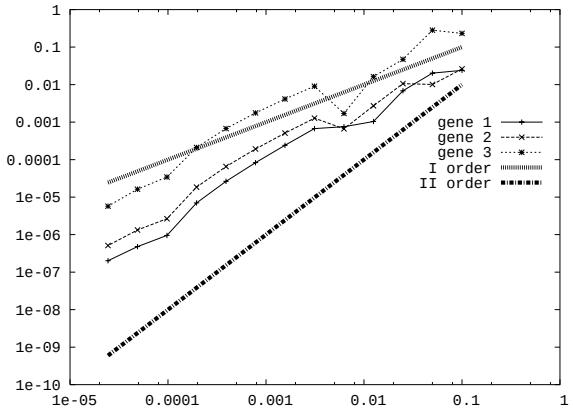

Figure 4.2: Convergence behaviour for the different genes.

This lack of smoothness causes order reduction from two to one for the standard second-order spatial discretization procedure. As an application we considered a model for simulating regulatory networks and numerically verified that it is capable of quantitatively reproducing spatial and temporal expression patterns in developmental processes.

In the model considered in Section 4 we utilized the specific features of the test case (*Drosophila*). Since at the early developmental stage of the *Drosophila* cells are not yet formed (no membrane), we defined equations (4.3) in the whole domain (diffusion through the cells). The specific geometry of the *Drosophila* embryo allowed us to reduce the three-dimensional model to a (pseudo) one-dimensional model. However, in other developmental processes (sponges, corals) cells are formed right away and possibly move through the body. It is also quite common that only some of the gene products diffuse through the organism. In that case equations (4.3) should be defined only in the extracellular space resulting in a very complex and possibly time-dependent domain but then the singular source terms are replaced by boundary conditions. It might also be necessary to consider two-dimensional or even three-dimensional models. Adding these features to the model and the numerical implementation is a big challenge.

Another aim of future work is to design numerical methods with a convergence order higher than one for the diffusion-reaction problems with singular source terms.

Acknowledgement We acknowledge support from the Dutch BSIK/BRICKS project and from NWO's 'Computational Life Science' program, projectnr. 635.100.010.

References

1. M. Ashyraliyev, J.G. Blom, and J.A. Kaandorp. A note on modelling developmental regulatory networks. Report MAS-R05xx, CWI, Amsterdam, 2005.
2. M.D. Greenberg. *Application of Green's Functions in Science and Engineering*. Prentice-Hall, New Jersey, 1971.
3. Vitaly V. Gursky, John Reinitz, and Alexander M. Samsonov. How gap genes make their domains: An analytical study based on data driven approximations. *CHAOS*, 11:132–141, 2001.
4. E. Hairer, C. Lubich, and G. Wanner. *Geometric Numerical Integration. Structure Preserving Algorithms for Ordinary Differential Equations*, volume 31 of *Springer Series in Computational Mathematics*. Springer Verlag, Berlin, 2002.
5. W. Hundsdorfer and J.G. Verwer. *Numerical Solution of Time-Dependent Advection-Diffusion-Reaction Equations*, volume 33 of *Springer Series in Computational Mathematics*. Springer Verlag, Berlin, 2003.
6. Johannes Jaeger, Svetlana Surkova, Maxim Blagov, Hilde Janssens, David Kosman, Konstantin N. Kozlov, Manu, Ekaterina Myasnikova, Carlos E. Vanario-Alonso, Maria Samsonova, David H. Sharp, and John Reinitz. Dynamic control of positional information in the early *Drosophila* embryo. *NATURE*, 430:368–371, 2004.
7. Eric Mjolsness, David H. Sharp, and John Reinitz. A connectionist model of development. *J. Theor. Biol.*, 152:429–453, 1991.
8. John Reinitz and David H. Sharp. Mechanism of *eve* stripe formation. *Mechanisms of Development*, 49:133–158, 1995.
9. Isaac Salazar-Ciudad, Jordi Garcia-Fernandez, and Ricard V. Solé. Gene networks capable of pattern formation: From induction to reaction-diffusion. *J. Theor. Biol.*, 205:587–603, 2000.
10. N.M. Temme. *Special Functions, An Introduction to the Classical Functions of Mathematical Physcis*. John Wiley & Sons, Inc., New York, 1996.

11. N.M. Temme. Personal communication, 2005.
12. Anna-Karin Tornberg and Björn Engquist. Numerical approximations of singular source terms in differential equations. *J. Comput. Phys.*, 200:462–488, 2004.

Appendix

The exact solution of the problem of Example (2.2). In 2D an interesting test model used in [12] is the Poisson equation

$$-\Delta u = \delta(\Gamma, x, y)\,. \tag{5.1}$$

The source $\delta(\Gamma; x, y)$ denotes the Dirac delta function along a curve Γ defined by

$$\int_{\mathbb{R}^2} \delta(\Gamma; x, y)dxdy = \int_{\Gamma} d\gamma\,, \tag{5.2}$$

with co-ordinate γ on Γ. If Γ is a circle, $\Gamma := \{(x, y) \in \mathbb{R}^2 : |(x, y)| < r_0\}$, the solution of (5.1) is radial symmetric and equivalent with the solution of

$$\frac{1}{r}\frac{\partial}{\partial r}(r\frac{\partial u}{\partial r}) = 0, \qquad \text{for } r > r_0 \tag{5.3}$$

and

$$\int_{\overline{\Gamma}} \Delta u = -\int_{\overline{\Gamma}} \delta(\Gamma, x, y) \tag{5.4}$$

or, using Gauss' theorem and (5.2)

$$2\pi r\frac{\partial u}{\partial r} = -2\pi r_0. \tag{5.5}$$

Integration of the latter gives

$$u = -r_0 \ln r + A, \tag{5.6}$$

where the constant A can be determined using the continuity of the solution at Γ, so $A = u(r_0) - r_0 \ln \frac{1}{r_0}$, resulting in

$$u(r) = u(r_0) - r_0 \ln \frac{r}{r_0}. \tag{5.7}$$

The logarithmic growth discussed in Remark 2.3. Consider again the expression

$$w_k = \sum_{\text{odd}\, i,j=1}^{m} 1/\mu_{ij}\,, \qquad \mu_{ij} = h^{-2}\big(\sin^2\big(\frac{\pi ih}{2}\big) + \sin^2\big(\frac{\pi jh}{2}\big)\big)\,, \qquad h = \frac{1}{m+1}$$

for the numerical solution at the center point. To explain the logarithmic growth of w_k with m we denote $m' = (m+1)/2$ and let here $\mathcal{O}(1)$ represent appropriately encountered constants independent of m'. From the inequality

$$4/\pi^2 < \sin^2(x)/x^2 \le 1\,, \qquad 0 \le x \le \pi/2\,,$$

follows $i^2+j^2 < \mu_{ij} \le (i^2+j^2)(\pi^2/4)$ or $(4/\pi^2)(i^2+j^2)^{-1} \le (\mu_{ij})^{-1} < (i^2+j^2)^{-1}$. Let us suppose that the lower bound determines the growth such that

$$w_k = \frac{4}{\pi^2} \sum_{\text{odd}\, i,j=1}^{m} \frac{1}{i^2+j^2} + \mathcal{O}(1) = \frac{1}{\pi^2} \sum_{i,j=1}^{m'} \frac{1}{i^2+j^2} + \mathcal{O}(1)\,.$$

To estimate the sum we denote $f(x) = f(x,j) = 1/(x^2+j^2)$ and use Euler's summation formula with remainder R_0 [10, 11],

$$\sum_{i=1}^{m'} f(i) = \int_0^{m'} f(x)\,dx + \frac{f(0)+f(m')}{2} + R_0 = \frac{1}{j}\arctan\left(\frac{m'}{j}\right) + \frac{1}{2}\,\frac{1}{j^2} + \frac{1}{2}\,\frac{1}{m'^2+j^2} + R_0\,.$$

Next we sum over j. Then the arctan-term dominates and the other terms can be shown to be $\mathcal{O}(1)$, giving

$$\pi^2\, w_k = \sum_{j=1}^{m'} \frac{1}{j}\arctan\left(\frac{m'}{j}\right) + \mathcal{O}(1) = \sum_{j=1}^{m'} \frac{1}{j+1}\arctan\left(\frac{m'}{j+1}\right) + \mathcal{O}(1)\,.$$

Using again Euler's summation formula,

$$\pi^2\, w_k = \int_0^{m'} \frac{1}{1+x}\arctan\left(\frac{m'}{x+1}\right) dx + \mathcal{O}(1)\,,$$

which leads us to the logarithmic behavior. With partial integration we can rewrite the integral as

$$\log(m'+1)\arctan\left(\frac{m'}{m'+1}\right) + m' \int_0^{m'} \frac{\log(1+x)}{(x+1)^2+m'^2}\,dx + \mathcal{O}(1)\,.$$

Substituting $x+1 = m't$ in the integral term yields

$$\pi^2\, w_k = \log(m'+1)\arctan\left(\frac{m'}{m'+1}\right) + m' \int_{1/m'}^{(m'+1)/m'} \frac{\log(m't)}{t^2+1}\,dt + \mathcal{O}(1)\,,$$

so that, using $\arctan(1) = \int_0^1 \frac{1}{1+t^2}\,dt = \frac{\pi}{4}$, $\int_0^1 \frac{\log(t)}{t^2+1}\,dt = -\log(2)$, we get for $m \to \infty$

$$\pi^2\, w_k = \frac{\pi}{4}\log(m') + \log(m') \int_0^1 \frac{1}{t^2+1}\,dt + \int_0^1 \frac{\log(t)}{t^2+1}\,dt + \mathcal{O}(1) = \frac{\pi}{2}\log(m) + \mathcal{O}(1)\,.$$

The derived slope $(2\pi)^{-1}$ coincides with the computed slope in Figure 2.3, right plot.